

# Creating Chiral Surfaces for Enantioselective Heterogeneous Catalysis: *R,R*-Tartaric Acid on Cu(110)

M. Ortega Lorenzo, S. Haq, T. Bertrams, P. Murray,<sup>†</sup> R. Raval,\* and C. J. Baddeley<sup>‡</sup>

Leverhulme Centre for Innovative Catalysis and Surface Science Centre, Department of Chemistry, University of Liverpool, Liverpool L69 7ZD, United Kingdom

Received: June 28, 1999

One of the most successful ways of inducing enantioselectivity in a heterogeneous catalytic system is by the adsorption of chiral “modifier” molecules on the reactive metal surface. However, little is known about the nature of the active sites present on the modified metal surface and how such modifiers bestow chirality to an achiral metal surface. In this paper we report the behavior of *R,R*-tartaric acid adsorption on a Cu(110) surface using high-resolution surface analytical techniques. *R,R*-Tartaric acid is known to be an extremely successful modifier molecule for the enantioselective hydrogenation of methyl acetoacetate, the simplest  $\beta$ -keto ester, to the *R*-enantiomer of the product molecule methyl 3-hydroxybutyrate. A combination of low-energy electron diffraction (LEED), scanning tunneling microscopy (STM), and Fourier transform reflection–absorption infrared spectroscopy (FT-RAIRS) techniques has allowed us to demonstrate that a complicated adsorption phase diagram exists for this system. A rich variety of ordered overlayer structures are produced, in which preferred molecular forms, bonding and orientations of the chiral molecules are adopted, dependent on coverage, temperature and time. These different adlayers will clearly play a different role in the enantioselective reaction. Of particular interest is the fact that under certain conditions, the 2-dimensional order of the *R,R*-tartaric acid adlayer destroys all symmetry elements at the surface, leading to the creation of extended chiral surfaces! Such chiral surfaces may be an important factor in defining the active site in heterogeneous enantioselective reactions.

## 1. Introduction

The development of heterogeneous catalytic routes capable of the conversion of a prochiral reagent into just one of the two possible optical isomers of the product would have extremely beneficial implications for the pharmaceutical and chemical industries. In each case, it is extremely important to achieve highly pure optically active products since even ppm levels of the undesired enantiomer can have catastrophic consequences in physiological applications. Heterogeneous enantioselective catalysts would potentially be cheaper and provide greater ease of handling and separation than the present organic synthetic and homogeneous routes. At present, the two heterogeneous enantioselective reactions that have received the most attention are the hydrogenation of  $\alpha$ -keto esters over supported Pt catalysts and the hydrogenation of  $\beta$ -keto esters over supported Ni catalysts.<sup>1,2</sup> The most interesting feature of these systems is that enantioselective behavior is only induced if the catalysts are first modified by the adsorption of chiral “modifier” molecules. In the case of the Pt system, the most prevalent modifiers are the cinchona alkaloids, while in the Ni system,  $\alpha$ -hydroxy acids and  $\alpha$ -amino acids have both proved successful. However, one of the fundamental questions in this field still remains unanswered: how do modifiers bestow chirality to an achiral metal surface and what is the nature of the active sites present on the modified surfaces? So far, the formulation of a clear answer has been hampered by the sheer complexity of

the working catalyst system and, therefore, we have chosen to address this gap in understanding by studying the adsorption behavior of pure chiral modifiers on a defined single-crystal metal surface with high-resolution surface analytical techniques.<sup>3</sup> In this paper we report the behavior of *R,R*-tartaric acid adsorption on the 2-dimensionally anisotropic Cu(110) surface. *R,R*-Tartaric acid is known to be an extremely successful modifier molecule for the enantioselective hydrogenation of methyl acetoacetate (the simplest  $\beta$ -keto ester) to the *R*-enantiomer of the product molecule methyl 3-hydroxybutyrate<sup>4,5</sup> (Figure 1). A multidisciplinary approach has been utilized in order to identify the 2-dimensionally ordered phases produced by *R,R*-tartaric acid growth using low-energy electron diffraction (LEED) and scanning tunneling microscopy (STM), and to enable a molecular description of the adsorbed modifier, its intermolecular interactions, and molecular orientation to be formulated, Fourier transform reflection–absorption infrared spectroscopy (FT-RAIRS) was used.

We show that a complicated adsorption phase diagram, dependent on coverage, temperature and time, is produced for *R,R*-tartaric acid adsorption on the Cu(110) surface. A variety of ordered overlayer structures are produced in which preferred molecular forms, bonding, and orientations of the chiral molecules are adopted. This work reveals, for the first time, the complexities and dynamics of the chirally modified metal surface<sup>3</sup> and demonstrates that simple models to describe the behavior of heterogeneous enantioselective systems may not be enough.

## 2. Experimental Section

Two ultrahigh vacuum (UHV) chambers were used in this study. The first chamber contained facilities for FT-RAIRS,

\* To whom correspondence should be addressed. E-mail: raval@liv.ac.uk. Fax: +44 151 794 3589.

<sup>†</sup> Permanent address: IRC in Surface Science, Department of Chemistry, University of Manchester, Manchester M13 9PL, United Kingdom.

<sup>‡</sup> Present address: Department of Chemistry, University of St. Andrews, Fife KY16 9ST, United Kingdom.

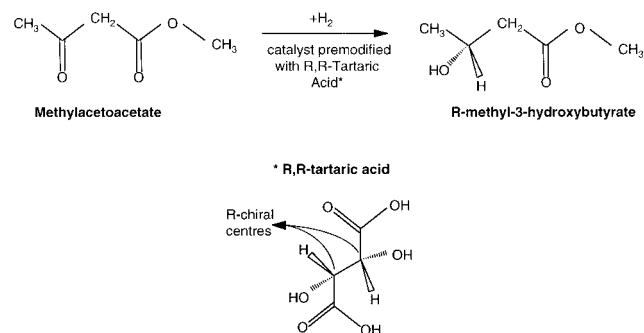


**Figure 1.** Asymmetric hydrogenation of methyl acetoacetate (MAA) to the *R*-enantiomer of the product molecule methyl 3-hydroxybutyrate ((*R*)-MHB) on a *R,R*-tartaric acid modified Ni catalyst.

TPD, LEED, and sample cleaning. This chamber was interfaced with a Mattson 6020 FT-IR spectrometer equipped with a liquid nitrogen cooled HgCdTe detector with a spectral range of 650–4000  $\text{cm}^{-1}$ . The second chamber was an Omicron Vakuumphysik STM chamber with facilities for STM, LEED, AES, and sample cleaning. All STM experiments were carried out with the sample at room temperature. The images were acquired in constant current mode.

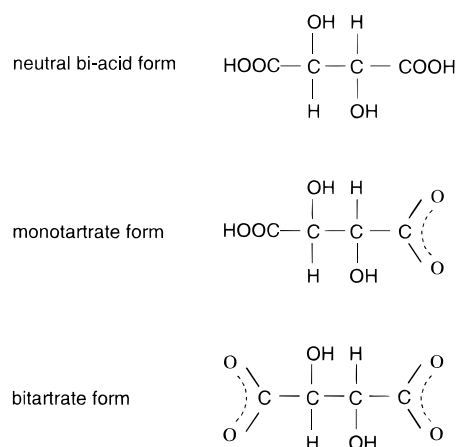
In each chamber, the Cu(110) crystal was cleaned by cycles of  $\text{Ar}^+$  ion sputtering, flashing, and annealing to 600 K. The surface ordering and cleanliness were monitored by LEED and AES. *R,R*-Tartaric acid (99%) was obtained from the Fluka Chemika Chemical Co. and was used without further purification. The acid was contained in a small resistively heated glass tube, separated from the main vacuum chamber by a gate valve, and differentially pumped by a turbo molecular pump. Before sublimation, the *R,R*-tartaric acid (TA) was outgassed at  $\sim 300$  K. The TA sample was then heated to  $\sim 370$  K and exposed to the copper crystal. During sublimation the main chamber pressure was typically  $2 \times 10^{-9}$  mbar.

RAIRS spectra were recorded throughout a continuous dosing regime as sample single beam infrared spectra and ratioed against a reference background single beam of the clean Cu(110) crystal. All spectra were obtained at 4  $\text{cm}^{-1}$  resolution with co-addition of 256 scans.

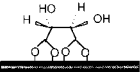
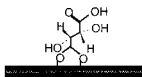
A CCD video camera interfaced to a computer was used for the digitization of the LEED patterns.

### 3. Results and Discussion

**3.1. *R,R*-Tartaric Acid.** *R,R*-Tartaric acid is a chemically versatile molecule, capable of existing in at least three different forms: the neutral bi-acid form, the monotartrate form where one of the carboxylic acid groups has deprotonated to give a carboxylate moiety, and the bitartrate form in which both acid groups have deprotonated (Figure 2). The chemistry of the molecule is further complicated by the fact that the intact carboxylic acid groups are capable of sustaining hydrogen bonds with other acid and alcohol groups, which potentially could lead to a number of intermolecular interactions.<sup>6</sup> Infrared spectroscopy provides a means of distinguishing between the different types of functional groups. For example, the carboxylate group is distinguished by the presence of the  $\nu_{\text{as}}(\text{COO})$  and  $\nu_{\text{s}}(\text{COO})$  vibrations at  $\sim 1600$  and  $1400$   $\text{cm}^{-1}$ , respectively, while the carboxylic acid group is indicated by distinct  $\nu(\text{C}=\text{O})$  and  $\nu(\text{C}-\text{O})$  vibrations at  $\sim 1750$  and  $1380$   $\text{cm}^{-1}$ , respectively.<sup>7</sup> Hydrogen-bonding interactions of the carboxylic acid groups lead to direct perturbations of the molecular vibrations, generally lowering the  $\nu(\text{O}-\text{H})$  and  $\nu(\text{C}=\text{O})$  stretches and increasing the



**Figure 2.** Three different forms in which tartaric acid molecules can exist.

405 K	 Bitartrate $\begin{pmatrix} 90 \\ 12 \end{pmatrix}$	High coverage monotartrate monolayer $\begin{pmatrix} 41 \\ 25 \end{pmatrix}$	Bi-acid multilayer
350 K	Monotartrate $\begin{pmatrix} 40 \\ 23 \end{pmatrix}$ ↓ slow change with time Bitartrate $\begin{pmatrix} 90 \\ 12 \end{pmatrix}$	High coverage monotartrate monolayer $\begin{pmatrix} 41 \\ 23 \end{pmatrix}$	
300 K	 Low coverage monotartrate monolayer $\begin{pmatrix} 40 \\ 23 \end{pmatrix}$		
83 K	Weakly perturbed neutral bi-acid molecules (HOOC-CHOH-CHOH-COOH)		

→ Increasing coverage

**Figure 3.** Adsorption phase diagram showing the molecular nature and two-dimensional order adopted by *R,R*-tartaric acid molecules on a Cu(110) surface as a function of coverage, temperature, and time.

$\nu(\text{C}-\text{O})$  vibrational frequencies.<sup>8–11</sup> Similarly, hydrogen-bonding of the alcohol groups leads to a downshift and band-broadening of the  $\nu(\text{O}-\text{H})$  stretch from the monomer value of  $\sim 3500$   $\text{cm}^{-1}$ . Whereas all these bands are easily identified at multilayer coverages, in the monolayer regime the  $\nu(\text{C}=\text{O})$  vibrational frequency proved to be the best indicator of an H-bonding interaction, since small bands arising from ice condensation on the cryogenically cooled detectors sometimes masked this spectral region and made it more difficult to unambiguously identify the adsorbate  $\nu(\text{O}-\text{H})$  vibration. Finally, using infrared spectroscopy in the reflection mode (RAIRS) allows orientation of functional groups at metal surfaces to be deduced by application of the dipole selection rule, which specifies that only those vibrations giving rise to a dynamic dipole moment perpendicular to the surface would be observed.<sup>12</sup>

Upon adsorption, the chemical complexities of tartaric acid described above are further compounded by the range of 2-dimensionally ordered structures that can be self-assembled at the surface. Therefore, to facilitate discussion, an adsorption phase diagram is shown in Figure 3, summarizing the molecular nature, ordered overlayer structures, and the characteristic bonding observed as a function of adsorption temperature and coverage when *R,R*-tartaric acid is adsorbed onto Cu(110). The 2-dimensionally ordered structures are described in matrix notation where the relationship between the metal surface net,

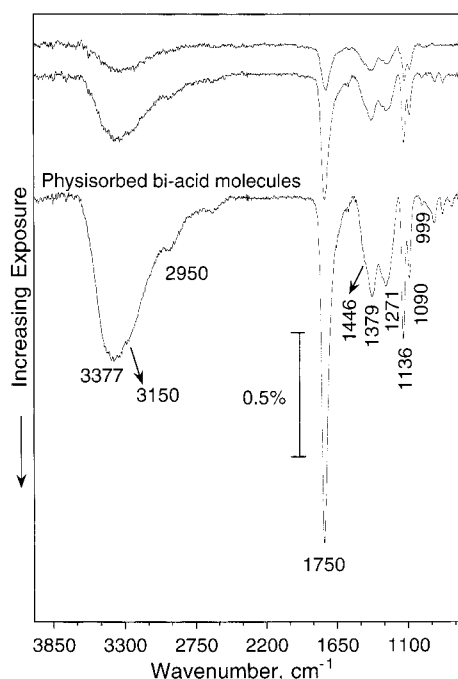


**Figure 4.** RAIR spectra observed as a function of increasing coverage of *R,R*-tartaric acid on Cu(110) at 83 K.

given by the vectors **a** and **b** and the overlayer net vectors **a'** and **b'** is given by

$$\begin{pmatrix} \mathbf{a}' \\ \mathbf{b}' \end{pmatrix} = \begin{pmatrix} G_{11} & G_{12} \\ G_{21} & G_{22} \end{pmatrix} \begin{pmatrix} \mathbf{a} \\ \mathbf{b} \end{pmatrix}$$

For convenience, the matrix formation shown above will be represented throughout in the text as  $(G_{11} \ G_{12}, \ G_{21} \ G_{22})$  where **a** is the unit vector along  $\langle 1\bar{1}0 \rangle$  and **b** is the unit vector along  $\langle 001 \rangle$ .

### 3.2. Low-Temperature Adsorption: The Molecular Phase.

Figure 4 shows the RAIR spectra obtained with increasing exposures of *R,R*-tartaric acid to the Cu(110) sample held at 83 K. There are no band position changes on going from the lowest exposures (submonolayer) to the highest exposures (multilayers). Furthermore, all the RAIRS bands observed show a strong similarity with the IR bands observed for solid *R,R*-tartaric acid<sup>13</sup> (Table 1), leading to the conclusion that, at these low temperatures, weakly perturbed neutral bi-acid molecules are adsorbed in the monolayer and in the multilayers formed on the Cu(110) surface. Solid tartaric acid possesses a complex H-bonded crystalline structure where intermolecular O—H...O hydrogen bonds between the acid groups of one molecule and acid and alcohol groups of nearby molecules create a 3-dimensional network of interactions.<sup>6</sup> The close correspondence between the RAIR spectra recorded here and the IR spectra of the crystalline structure (Table 1) suggests that a similar network of H-bonding interactions also exists for the adsorbed phase on Cu(110) at 83 K, giving rise to characteristic broad and downshifted  $\nu(\text{O—H})_{\text{alcohol}}$  bands between 3400 and 3200  $\text{cm}^{-1}$  and the  $\nu(\text{O—H})_{\text{acid}}$  bands at 3200–3000  $\text{cm}^{-1}$ . However, at no stage were any ordered LEED structures observed following *R,R*-tartaric acid adsorption at 83 K, indicating that no long range ordered structures are created at these low temperatures. Finally, IR data show that the multilayer desorbs from the surface at just below 330K.

### 3.3. Adsorption at 300 K: The Monotartrate Phases.

(i) *Low Coverage Adsorption.* Figure 5 outlines the main stages

of growth observed by STM when *R,R*-tartaric acid is adsorbed on Cu(110) at 300 K. Nucleation of *R,R*-tartaric acid islands occurs in the early stages of adsorption and is often located at step edges (Figure 5a). Increasing coverage leads to the steady growth of these islands (Figure 5b) until the entire surface is covered by this phase. Direct information on the molecular nature of the adsorbed species in the islands depicted in Figure 5a,b comes from the corresponding RAIRS data (Figure 6a,b), which reveal bands at 1711 and 1437  $\text{cm}^{-1}$ . The former band can be correlated with a C=O group,<sup>14</sup> while the latter is a strong indicator of the carboxylate group, which gives a  $\nu_s(\text{COO})$  vibration at this frequency.<sup>7</sup> It, therefore, seems that both the acid and the carboxylate groups are present in the adlayer, a situation that could arise from one of two possibilities: every molecule in the adlayer exists as a monotartrate species in which one end retains the acid functionality and the other deprotonates, or there is a coexistence of bi-acid and bitartrate molecules at the surfaces, the former retaining both acid functionalities and the latter undergoing a double deprotonation to give two carboxylate groups on the molecule. The presence of two different species coexisting at the surface is rejected on the basis that the bitartrate species gives rise to very distinctive IR spectral features that are missing from all spectra shown in Figure 6. In addition, thermal programmed desorption (TPD) data<sup>23</sup> from this adlayer are dominated by a sharp desorption peak at 483 K, which is much higher than the desorption temperature of below 250 K observed for the bi-acid molecules created at the surface when adsorption is carried out at low temperatures. We, therefore, conclude that the spectra in Figure 6 correspond to strongly adsorbed monotartrate species and a detailed assignment of the IR bands is given in Table 1. We note that the carboxylate group provides strong bonding interaction with the metal surface as, for example, observed in the formate,<sup>15</sup> acetate,<sup>16</sup> benzoate,<sup>17</sup> and alanine<sup>18</sup> species, and must serve a similar function in strongly anchoring the monotartrate species to the surface, leading to the high desorption temperature. Application of the infrared metal surface selection rule<sup>12</sup> allows the orientation adopted by this functionality to be determined; the presence of the  $\nu_s(\text{COO})$  vibration at 1437  $\text{cm}^{-1}$  but the absence of the usually strong  $\nu_{\text{as}}(\text{COO})$  vibration expected in the 1550–1650  $\text{cm}^{-1}$  range implies that the two O atoms in the carboxylate group are equidistant from the surface, rendering the latter vibration inactive, but retaining the dipole activity of the  $\nu_s(\text{COO})$  vibration. Turning to the acid end of the monotartrate species, we note that the frequency of the  $\nu(\text{C=O})$  vibration in the monotartrate species is 1711  $\text{cm}^{-1}$ , which is downshifted from the multilayer value and is much lower than observed for monomeric carboxylic acids,<sup>19,20</sup> consistent with the presence of considerable H-bonding in the adlayer. This type of intermolecular interaction explains why *R,R*-tartaric acid shows a strong tendency to form islands at low coverage (Figure 5a,b).

Information on the self-organization of the monotartrate units in the islands depicted in Figure 5a,b is provided by LEED and STM studies. LEED data obtained during this adsorption stage reveal a good  $c(4 \times 6)$ , or in matrix notation  $(4 \ 0 \ 2 \ 3)$ , LEED pattern which, after a few seconds of exposure to the LEED beam or gentle annealing, converts to a  $c(4 \times 2)$  or  $(4 \ 0 \ 2 \ 1)$  structure (Figure 7a). Throughout this adsorption stage, STM images reveal that the local packing order within the islands remains the same, composed of identical individual features that take up a  $(4 \ 0 \ 2 \ 1)$  arrangement (Figure 7b). The  $(4 \ 0 \ 2 \ 3)$  structure was much more difficult to detect by STM and was only imaged occasionally when an adsorbed island was scanned for the first time, showing every third feature giving rise to a



**TABLE 1: Characteristic Vibrational Bands ( $\text{cm}^{-1}$ ) and Assignments of the Various Phases Formed by *R,R*-Tartaric Acid Adsorbed on Cu(110) in Comparison with Solid Tartaric Acid and Anhydrous Rochelle Salt<sup>b</sup>**

TA powder <sup>13</sup> ( $\text{cm}^{-1}$ , assignment)		anhydrous Rochelle salt <sup>b</sup> powder <sup>22</sup> ( $\text{cm}^{-1}$ , assignment)		RAIRS data for biacid/Cu(110) ( $\text{cm}^{-1}$ , assignment) (this work)		RAIRS data for monotartrate in the (4 0, 2 3) structure ( $\text{cm}^{-1}$ , assignment) (this work)		RAIRS data for bitartrate in the (9 0, 1 2) structure ( $\text{cm}^{-1}$ , assignment) (this work)	
3388 br, s, 3315 br, s	$\nu_{\text{OH}}^{\text{alc}}$	3304 br, s	$\nu_{\text{OH}}^{\text{alc}}$	3377 br, s	$\nu_{\text{OH}}^{\text{alc}}$				
3193 br, s, 3083 br, s	$\nu_{\text{OH}}^{\text{acid}}$			3150 br, s	$\nu_{\text{OH}}^{\text{acid}}$				
2972 br, 2939 br	$\nu_{\text{C-H}}$	2983 br, 2939 br	$\nu_{\text{C-H}}$	2950 br	$\nu_{\text{C-H}}$				
1741 br, vs	$\nu_{\text{C=O}}$			1750 s	$\nu_{\text{C=O}}$	1711 s	$\nu_{\text{C=O}}$		
1453 br, s	$\nu_{\text{C-O}}^{\text{acid}}$	1594 br, s	$\nu_{\text{asym}}(\text{OCO})$	1446 so	$\nu_{\text{C-O}}^{\text{acid}}$				
		1433 s, 1411 s	$\nu_{\text{sym}}(\text{OCO})$			1437 s	$\nu_{\text{sym}}(\text{OCO})$	1430 sh, s, 1410 sh, s	$\nu_{\text{sym}}(\text{OCO})$
1375 s	$\delta_{\text{OH}}^{\text{alc}}$	1380 s, 1344 w	$\delta_{\text{OH}}^{\text{alc}}$	1379 br	$\delta_{\text{OH}}^{\text{alc}}$	1398 w, 1378 w, so	$\delta_{\text{OH}}^{\text{alc}}$	1375 so	$\delta_{\text{OH}}^{\text{alc}}$
1318 w, 1255 m, 1220 m	$\delta_{\text{OH}}^{\text{acid}}$ + $\delta_{\text{CH}}$	1312 w, 1245 vw, 1211 vw	$\delta_{\text{CH}}$	1271 br	$\delta_{\text{OH}}^{\text{acid}}$ + $\delta_{\text{CH}}$	1338 w, 1300 w, 1234 m, 1197 w	$\delta_{\text{OH}}^{\text{acid}}$ + $\delta_{\text{CH}}$	1338 s, 1200 w	$\delta_{\text{CH}}$
1190 m, 1134 m, 1087 m	$\nu_{\text{C-O}}^{\text{alc}}$	1113 w, 1069 w	$\nu_{\text{C-O}}^{\text{alc}}$	1136 m, 1090 m	$\nu_{\text{C-O}}^{\text{alc}}$	1101 m	$\nu_{\text{C-O}}^{\text{alc}}$	1113 s	$\nu_{\text{C-O}}^{\text{alc}}$
992 w	$\nu_{\text{C-C}}$	994 w	$\nu_{\text{C-C}}$	999 vw	$\nu_{\text{C-C}}$			999	$\nu_{\text{C-C}}$

<sup>a</sup> s, m, w, v, sh, br and sh indicate strong, medium, weak, very, sharp, broad, and shoulder, respectively. <sup>b</sup> Anhydrous Rochelle Salt:  $\text{Na}^+\text{K}^+[\text{COO}(\text{HO})\text{HCCH}(\text{OH})\text{COO}^{2-}]$ .

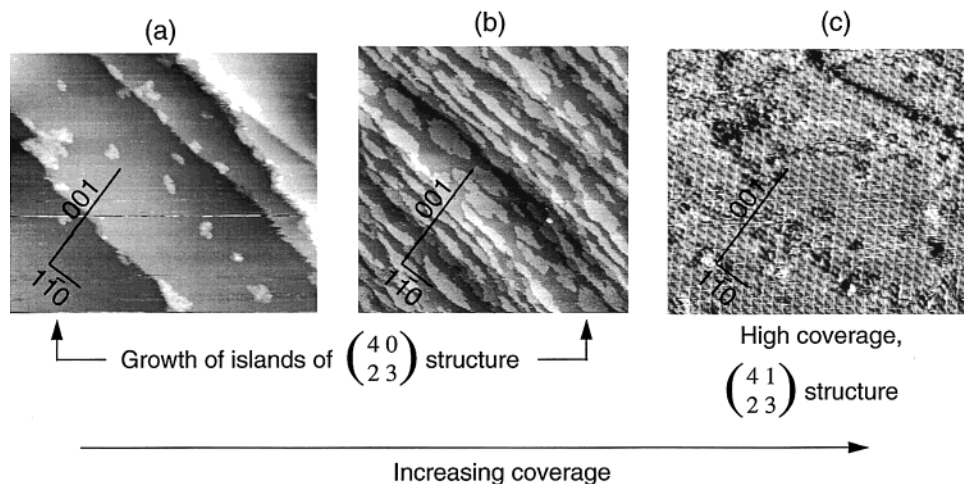


**Figure 5.** STM images showing the main stages of growth observed when *R,R*-tartaric acid is adsorbed on Cu(110) at 300 K. STM images (a) ( $500 \times 500 \text{ \AA}$ ) [ $I_t -2.05 \text{ V}$ ;  $V_{\text{tip}} 0.46 \text{ nA}$ ] and (b) ( $1000 \times 1000 \text{ \AA}$ ) [ $V_{\text{tip}} -1.90 \text{ V}$ ;  $I_t 0.46 \text{ nA}$ ] show the formation of (4 0, 2 3) islands with increasing coverage. Image (c) ( $300 \times 300 \text{ \AA}$ ) [ $V_{\text{tip}} -1.1 \text{ V}$ ;  $I_t 0.46 \text{ nA}$ ] shows the high coverage (4 1, 2 3) monolayer.

different contrast. A repeat scan of the same area generally always resulted in the observation of the (4 0, 2 1) structure with all STM features giving rise to a similar contrast in the image. Clearly, the conversion of the (4 0, 2 3) structure into the (4 0, 2 1) structure, observed under the LEED beam, also occurs with equal facility during tunneling experiments. Interestingly, both STM structures show the same packing of individual features separated by  $\sim 7.2 \text{ \AA}$  along the  $\langle 001 \rangle$  direction and  $\sim 6.3 \text{ \AA}$  along the  $\langle 111 \rangle$  direction (Figure 7b). The maximum length that could be associated with the *R,R*-tartaric acid is when the three C—C bonds and the two COOH groups lie in the same plane, at which point the two ends of the molecule would be  $\sim 5 \text{ \AA}$  apart. This length is much smaller than the repeat distances observed by STM and, from this argument, each individual feature in the STM images must arise from a separate molecule. This implies a local coverage of 0.25 monolayer in both the (4 0, 2 1) and (4 0, 2 3) structures. It is clear that these

two structures are closely related with identical adsorption arrangements except that, essentially, the (4 0, 2 3) structure is a lower symmetry manifestation of the (4 0, 2 1) structure. We note that in both adlayers, the nearest neighbor molecules are separated by  $6.26 \text{ \AA}$ , a distance that allows the acid group of one molecule to approach the OH group of the neighboring molecule closely enough for H-bonding interactions to occur<sup>13</sup> (Figure 8a). In fact, the presence of considerable H-bonding in the adlayer is confirmed by the downshifted  $\nu(\text{C=O})$  in the RAIRS data (Figure 6a,b). At present we, therefore, attribute the difference in symmetry of the two adlayers to differences in the intermolecular H-bonding networks (Figure 8b). The symmetry of the (4 0, 2 1) structure demands that all the molecules remain identical, so we propose that the intermolecular H-bonds leads to a network consisting of straight chains aligned along the  $\langle 111 \rangle$  direction. In the (4 0, 2 3) structure, we propose that a different 2-dimensional network is created in

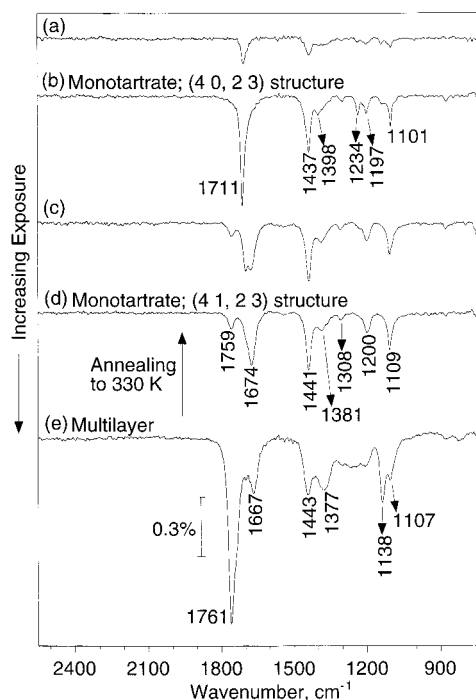


**Figure 6.** RAIR spectra observed as a function of increasing coverage of *R,R*-tartaric acid adsorbed on Cu(110). Spectra shown in (a), (b), and (d) were obtained at 300 K while (c) and (e) were obtained at 350 K.

which a “kinked” H-bonded unit occurs at every third molecule in the chain, thus reducing the symmetry of the adlayer. The distances between molecules involved in the “straight” or “kinked” H-bond are identical, so the (4 0, 2 3) structure could be readily converted to the (4 0, 2 1) structure simply by a concerted switch in direction of every third H-bond from the kinked orientation to the straight one (Figure 8b).

(ii) *High Coverage Adsorption.* Once the surface is effectively covered in the (4 0, 2 3)/(4 0, 2 1) phase, further adsorption leads to the creation of a new high coverage ordered phase, which is stable over the temperature range 300–400 K (Figure 3). The LEED data indicate the onset of this transition with streaking along the direction between the  $(-1, 0)$  and  $(\frac{1}{2}, -1)$  spots in the LEED pattern, finally resulting in a (4 1, 2 3) LEED pattern at high coverage, as shown in Figure 9b. STM images of this phase exhibit a very ordered adlayer, also with a (4 1, 2 3) repeat structure (Figure 5c). The RAIRS data of this (4 1, 2 3) phase (Figure 6d) retain the overall fingerprint of the monotartrate species; however, important clues on the altered nature of this adlayer come from the direct perturbation of the  $\nu(\text{C}=\text{O})$  band at  $1711\text{ cm}^{-1}$  of the original monotartrate species (Figure 6b), leading to the evolution of two new bands at  $1759$  and  $1674\text{ cm}^{-1}$ . This band splitting is observed most clearly when adsorption is carried out at 380 K (Figure 6c). With increasing coverage at 300 K, the  $1759\text{ cm}^{-1}$  band associated with the (4 1, 2 3) structure is submerged under contributions from the multilayer phase (Figure 6e). These data, collectively, suggest that the (4 1, 2 3) phase is produced by the accommodation of some more molecules in the first layer at the surface. Interestingly, the perturbation caused by this increase in coverage is felt most strongly by the acid groups of the monotartrate species with the emergence of two different  $\nu(\text{C}=\text{O})$  bands at  $1759$  and  $1674\text{ cm}^{-1}$ , indicating that two types of acid groups now exist in this phase: the latter frequency typical of H-bonded cyclic acid dimers<sup>19,20</sup> that lead to a strong downshift in frequency and the former indicative of a monomer

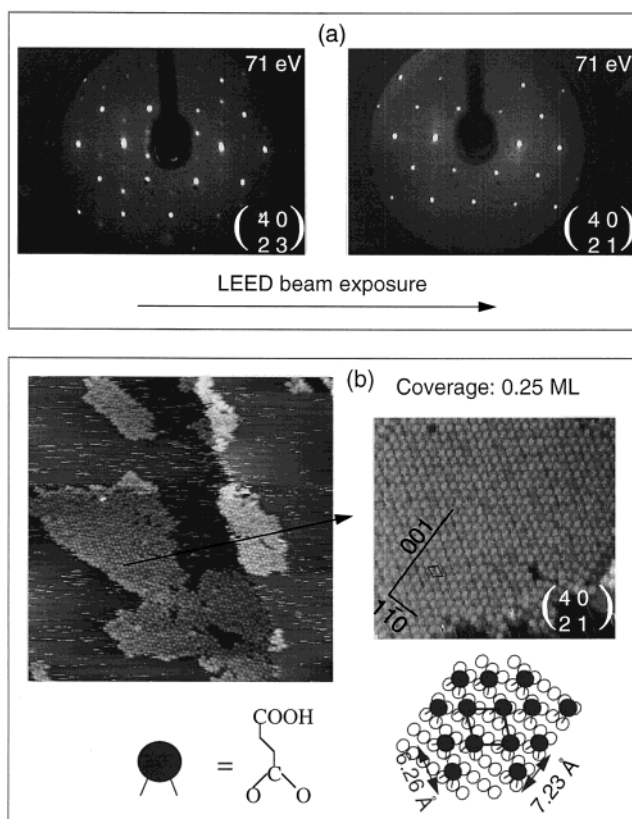


**Figure 7.** (a) (4 0, 2 3) LEED pattern observed at low coverage of *R,R*-tartaric acid on Cu(110) at 300 K, and its conversion to a (4 0, 2 1) arrangement after a few seconds of LEED beam exposure. (b) STM images ( $400 \times 400\text{ Å}$ ) [ $V_{\text{tip}} -1.96\text{ V}$ ;  $I_t 0.46\text{ nA}$ ] and ( $175 \times 160\text{ Å}$ ) [ $V_{\text{tip}} -1.52\text{ V}$ ;  $I_t 1.25\text{ nA}$ ] of islands of (4 0, 2 1) phase formed by *R,R*-tartaric acid adsorption on Cu(110) at 300 K. A schematic of the adlayer is shown where each monotartrate molecule is placed so that the carboxylate unit occupies a short-bridged site that places each oxygen above a Cu atom.<sup>15</sup>

or open-chain acid group that involves less H-bonding. In contrast, the  $1437\text{ cm}^{-1}$  vibrational band due to the carboxylate functionality anchored to the Cu(110) remains almost unaltered throughout the creation of this phase, indicating that this part of the adlayer is essentially similar to that of the (4 0, 2 3)/(4 0, 2 1) phases.

Using the chemical information above and data from STM images taken at different tunneling conditions, a model of the (4 1, 2 3) adlayer can be constructed as follows. STM images in Figure 10a–c show that along the  $\langle 001 \rangle$  direction, repeat units consisting of a bright two-lobed structure and a smaller feature are seen. The two-lobed structures are held  $\sim 18.0\text{ Å}$  apart along the  $\langle 001 \rangle$  direction with the smaller feature placed in between. Each two-lobed structure is  $\sim 7.2\text{ Å}$  in length and is observed to stack parallel to others in chains along the  $\langle 1\bar{1}2 \rangle$  direction. Again, using the fact that the maximum length a monotartrate molecule can project along the surface is  $5\text{ Å}$ , we attribute the two-lobed structure as arising from two adsorbed molecules and the smaller feature as arising from a single adsorbed molecule. On this basis, the schematic adlayer in Figure 10d can be constructed, which clearly possesses the (4 1, 2 3) repeat unit, with a coverage of 0.3 monolayer. In addition, we note that, under certain tunneling conditions, the STM pictures of the (4 1, 2 3) structure show a complex structure interconnected by lines along the  $\langle 1\bar{1}2 \rangle$  and  $\langle 1\bar{1}0 \rangle$  axes (Figure 10b,e). Finally, in Figure 10 c, we show an inverted STM image that essentially

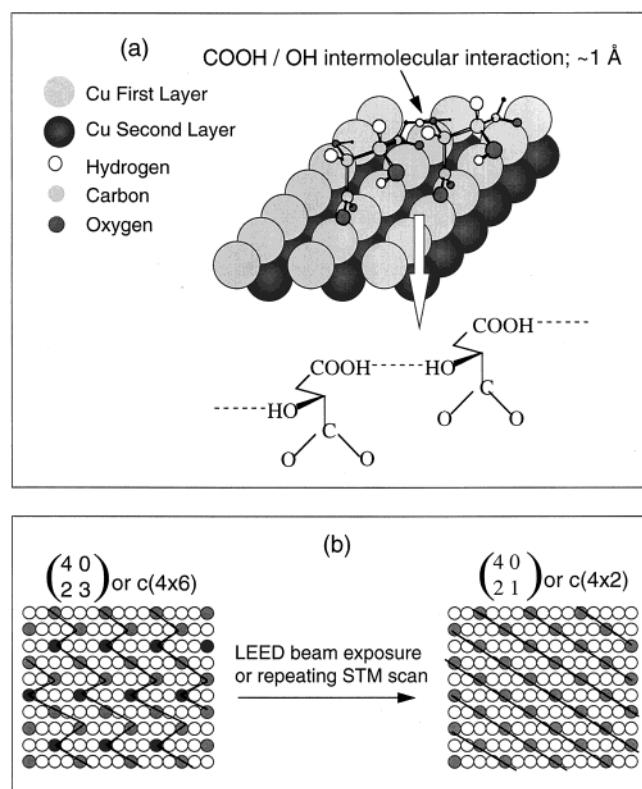


**Figure 8.** (a) Depiction of intermolecular hydrogen-bonding interactions between neighboring monotartrate molecules. (b) Proposed intermolecular H-bonding networks for the (4 0, 2 3) and (4 0, 2 1) coverages.

reveals the “empty” spaces in the molecular adlayer, depicted in Figure 10f.

The RAIRS data for this structure allow more chemical detail to be added to the schematic adlayer shown in Figure 10d, which helps to rationalize the STM data in Figure 10b and the directions of growth of the doublet chain structure. First, it is

clear from the vibrational data that cyclic carboxylic acid dimers and monomer acid groups coexist in this structure. It can be seen that the molecules giving rise to the two-lobed STM features are closely placed in this structure and we propose that this proximity leads to the formation of intermolecular cyclic acid dimer units (Figure 11b), explaining the emergence of the strong  $\nu(\text{C}=\text{O})$  band at  $1667\text{ cm}^{-1}$  in Figure 6 d. In addition, Figure 11b shows that each cyclic dimer unit possesses two OH groups, one at each end; H-bonding interactions between the OH groups of adjacent dimer units would naturally force the dimer chain along  $\langle 1\bar{1}2 \rangle$  direction. It is interesting to note that the STM image in Figure 10b also shows strong lines along the  $\langle 1\bar{1}2 \rangle$  direction, which coincides with the alignments that need to be adopted by these dimer OH groups in order to facilitate strong H-bonding intermolecular interactions. In addition, this STM image shows that similar direct lines are also observed along the  $\langle 1\bar{1}0 \rangle$  direction, suggesting that the OH groups on the single monotartrate molecules are also involved in H-bonding with the adjacent dimer units. Such interactions would essentially weave the entire structure together by connecting neighboring dimer chains. Here, the juxtaposition of the OH groups in the single molecules with the free OH groups of the dimer allows such a H-bonding connection to be easily made along the  $\langle 1\bar{1}0 \rangle$  direction (Figure 11c). It should be noted that in such a structure the acid group of the single monotartrate molecules remains free, rationalizing the emergence of the additional  $\nu(\text{C}=\text{O})$  band at  $1757\text{ cm}^{-1}$  (Figure 6d).

**3.4. Adsorption at 405 K: The Appearance of the Bitartrate Phase.** (i) *Low Coverage Adsorption.* The RAIR spectra for *R,R*-tartaric acid adsorption at 405 K are shown in Figure 12. The spectra observed at low coverage, e.g., Figure 12a, show an almost complete absence of the  $\nu(\text{C}=\text{O})$  band in the  $1700\text{ cm}^{-1}$  wavenumber range in contrast to the strong signals observed in the monotartrate phases. Changes are also observed for the carboxylate  $\nu_s(\text{COO})$  vibration region where the single  $1437\text{ cm}^{-1}$  band of the monotartrate is replaced by two closely spaced bands at  $1430$  and  $1410\text{ cm}^{-1}$  (Figure 12a). Finally, changes are also observed in the  $1101$  and  $1338\text{ cm}^{-1}$

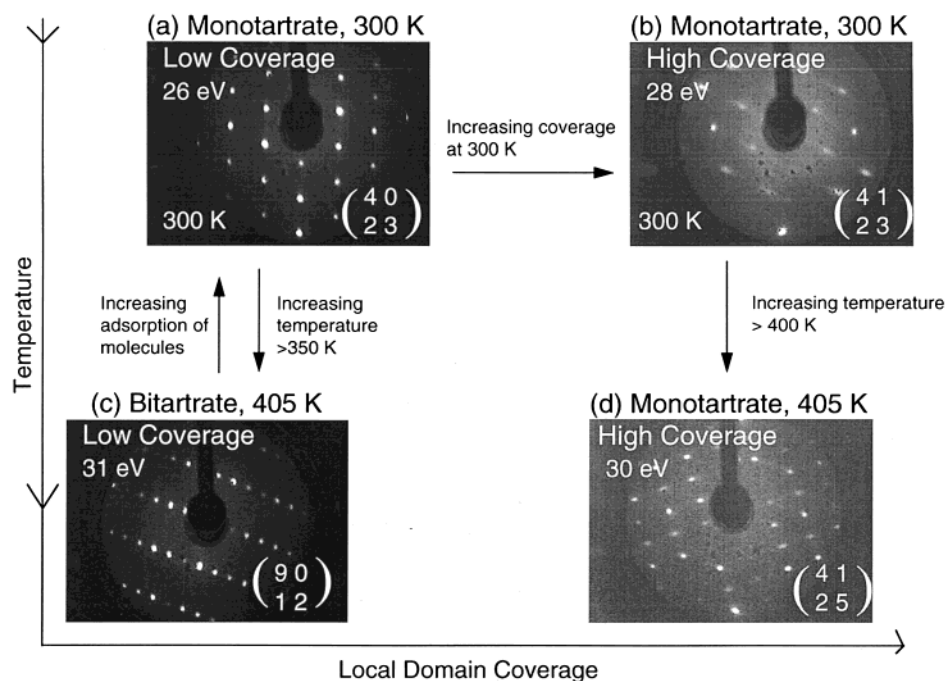


**Figure 9.** LEED patterns observed for *R,R*-tartaric acid adsorbed on Cu(110), as a function of coverage and temperature, showing (a) the (4 0, 2 3), (b) the (4 1, 2 3), (c) the (9 0, 1 2), and (d) the (4 1, 5 2) structures.



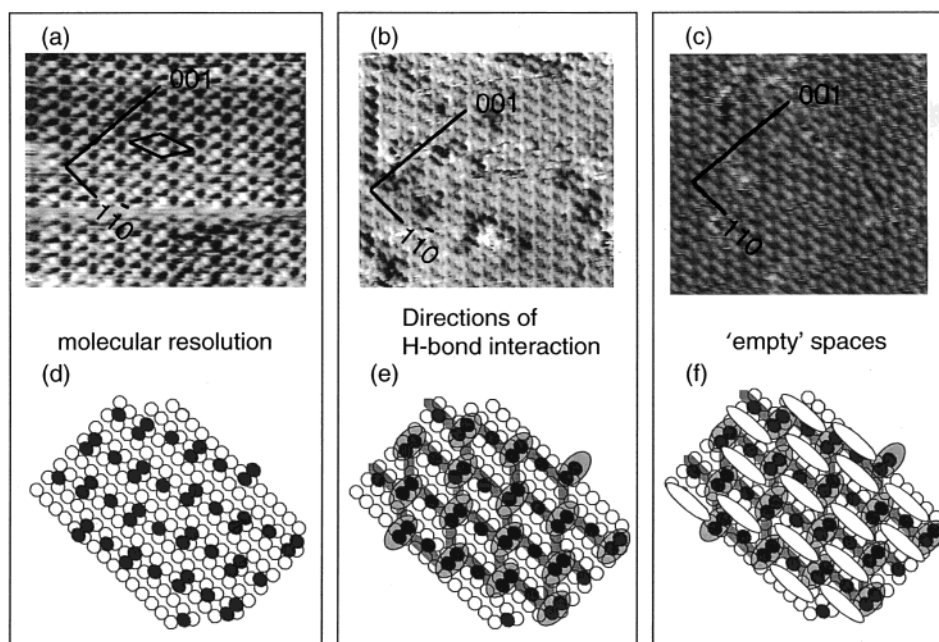


**Figure 10.** STM images of the (4 1, 2 3) structure taken at different tunneling conditions. (a) Molecular resolution showing the position of the adsorbed *R,R*-TA molecules ( $150 \times 150$  Å) [ $V_{\text{tip}} -0.03$  V;  $I_t$  0.51 nA]. (b) Lines along the  $\langle 112 \rangle$  and  $\langle 1\bar{1}0 \rangle$  directions coinciding with the positions that would have to be adopted by OH groups in order to create a network of H-bonds between molecules ( $150 \times 150$  Å) [ $V_{\text{tip}} -1.11$  V;  $I_t$  0.46 nA]. (c) Inverted image to outline empty spaces in the molecular adlayer ( $150 \times 150$  Å) [ $V_{\text{tip}} -1.37$  V;  $I_t$  0.61 nA].

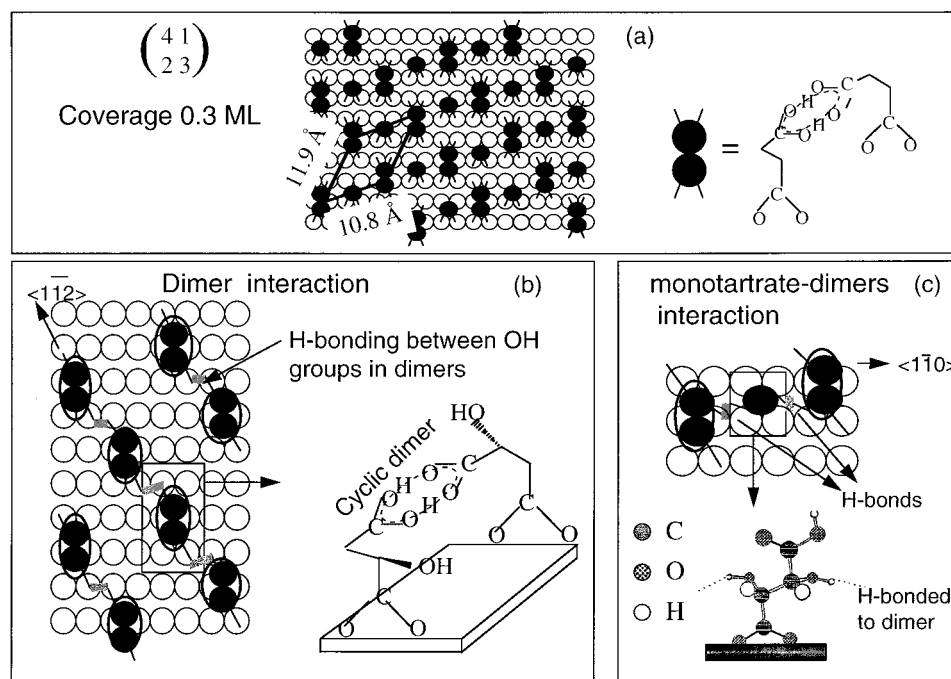


**Figure 11.** (a) Schematic diagram showing the unit cell and the position of the *R,R*-tartaric acid molecules in the (4 1, 2 3) structure. (b) Formation of cyclic dimers and the hydrogen-bonding interaction between dimers along the  $\langle 112 \rangle$  direction. (c) Depiction of single monotartrate molecules involved in further H-bonding interactions along the  $\langle 1\bar{1}0 \rangle$  direction, thus weaving dimer chains together. Note that in all structures the carboxylate groups bonding with the surface are placed in short-bridged sites, which places each oxygen above a Cu atom.<sup>15</sup>

bands, which both increase in relative intensity and sharpen compared to the monotartrate phase at 300 K. A comparison of this spectrum with the IR spectra of dipotassium tartrate<sup>21</sup> and Rochelle salt,<sup>22</sup> in which the tartaric acid is bound as a bitartrate ion, shows a remarkable correspondence, suggesting that at high temperatures the formation of a bitartrate species occurs directly upon initial adsorption. The presence of a bitartrate species also explains why the RAIR spectra contain no  $\nu(\text{C}=\text{O})$  peak. Detailed assignments of all the bands observed in this phase are shown in Table 1. It can be seen that  $\nu_s(\text{COO})$  gives rise to

a doublet band, an effect also observed for bitartrate salts<sup>21,22</sup> and attributed to either the coupling of the two identical COO oscillators on each molecule<sup>13</sup> or to the presence of two inequivalent adsorption sites for the bidentate molecules on the surface. Again, the application of the RAIRS selection rule allows one to determine that the two oxygen atoms in each COO unit are held almost equidistant from the surface, thus significantly attenuating the  $\nu(\text{COO})_{\text{as}}$  vibration.

The increase in relative intensity of the bands at 1338 and 1113  $\text{cm}^{-1}$ , corresponding to the  $\delta(\text{C}-\text{H})$  and  $\nu(\text{C}-\text{OH})$

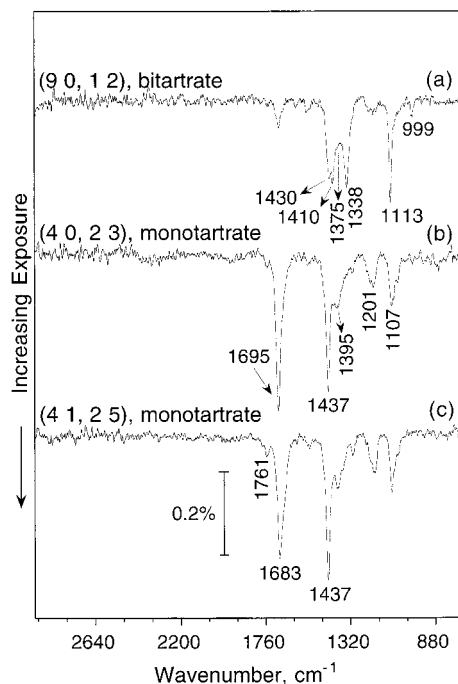


**Figure 12.** RAIR spectra observed as a function of increasing coverage of *R,R*-tartaric acid adsorbed on Cu(110) at 405 K.

vibrations respectively, can be rationalized in terms of the geometry of the bitartrate species (Figure 13b), in which the two carboxylate ends of the molecule are bonded to the surface, leaving the C2–C3 bond almost parallel to the surface. This geometry means that the C–OH bond is now more directed toward the surface normal compared to the monotartrate species (Figure 8a) while the C–H bond, which was almost vertical in the monotartrate species, adopts a new geometry more directed toward the surface parallel. This would give rise to the observed strong dipole activity of the  $\delta(\text{C–H})$  and  $\nu(\text{C–OH})$  vibrations (Table 1).

The bitartrate phase created at high temperatures also exhibits very significant 2-dimensional order, giving rise to a good LEED pattern (Figure 9c), which can be indexed in matrix notation as  $(9\ 0, 1\ 2)$ . STM images (Figure 13a) confirm the presence of this repeat unit cell and show that two other extra molecules exist per unit cell, resulting in a local coverage of 0.17 monolayer. The bitartrate molecules are arranged in rows of three, measuring a length of  $\sim 12\ \text{\AA}$ . A schematic diagram showing the approximate position of the molecules on the Cu-(110) surface is shown in Figure 13b. Since the carboxylate unit has been shown<sup>15</sup> to exhibit a strong preference for the bridge site on the close-packed Cu(110) rows, each bitartrate molecule is placed so that it straddles the Cu rows allowing both carboxylate ends of the molecule to bond in such a preferred manner. It can be noted from the STM image and from its correspondent LEED pattern that the bitartrate species form chains along the  $\langle 1\bar{1}4 \rangle$  surface direction. As for the other structures, we attribute this chain alignment to the close proximity of neighboring molecules that participate in intermolecular H-bonding interactions whose direction is dictated solely by the conformation of the  $\alpha$ -hydroxy groups on the bitartrate species (Figure 13b). The rigid adsorption geometry and the chirality of the *R,R*-tartaric acid molecules preserves this conformation so that no other rotational domain is created. It is interesting to note that this fact combined with the fact that the chain growth direction breaks all the symmetry elements of the underlying metal, means that we have created an *extended chiral surface*! In other words, the self-organization of the chiral molecules has allowed chirality to be directly bestowed onto the achiral metal surface. We note that for the same reasons as outlined for the  $(9\ 0, 1\ 2)$  structure, the  $(4\ 1, 2\ 3)$  structure created at 300 K also represents an extended chiral surface.

(ii) *High Coverage.* As the coverage is increased, the IR spectra associated with the bitartrate form disappears and are replaced by spectra that bear a close resemblance to those observed for the  $(4\ 0, 2\ 3)$  and the  $(4\ 1, 2\ 3)$  structures at 300 K (Figure

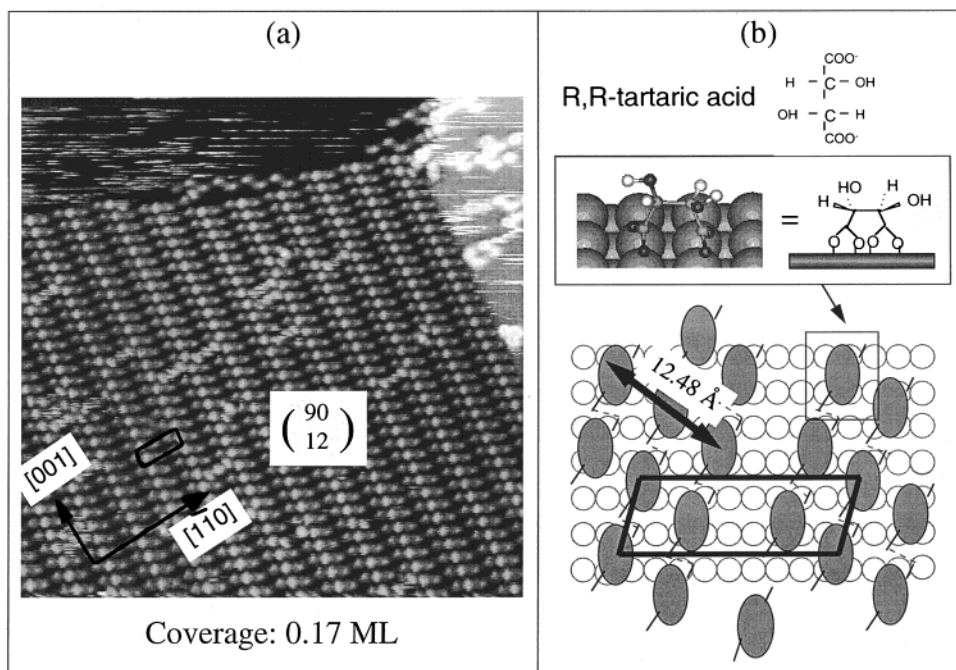


**Figure 13.** Depiction of the  $(9\ 0, 1\ 2)$  bitartrate phase. (a) STM image ( $200 \times 200\ \text{\AA}$ ) [ $V_{\text{tip}} = 1.7\ \text{V}$ ;  $I_t = 1.18\ \text{nA}$ ] showing the  $(9\ 0, 1\ 2)$  phase formed by *R,R*-tartaric acid adsorption on Cu(110) at 405 K. (b) Schematic diagram showing the position of the features observed in the STM image relative to the Cu(110) surface. H-bonds between  $\alpha$ -hydroxy groups on bitartrate molecules along the  $\langle 1\bar{1}4 \rangle$  surface direction are drawn as dotted lines. The bonding and orientation of the adsorbed bitartrate species on the Cu(110) surface are also shown.



13b,c), which are associated with the monotartrate species. This clearly suggests that upon increasing adsorption, the bitartrate form becomes unstable with respect to the monotartrate form,<sup>23</sup> which then dominates the adlayer. The high-coverage LEED pattern observed at 405 K and above, associated with the IR spectrum in Figure 12, is slightly different from that at 300 K, being indexed as (4 1, 2 5) (Figure 9d). This LEED pattern is also achieved by heating the (4 1, 2 3) structure to above 405 K. As no desorption is observed in this heat treatment, we must assume that the coverage in the (4 1, 2 5) structure is similar to that in the (4 1, 2 3) structure (i.e., ~0.3 monolayer). In addition, the strong similarity in the IR spectra of the two structures suggests that the dimer and single molecule units of the (4 1, 2 3) structures must prevail in the (4 1, 2 5) structure.

#### 4. Conclusions and Implications for Enantioselective Heterogeneous Catalysis

In summary, we conclude that the interaction of *R,R*-tartaric acid with a Cu(110) surface produces a complex adsorption phase diagram (Figure 3), where the chemical identity and 2-dimensional order of the adsorbed species varies significantly as a function of coverage and temperature. At very low temperatures the bi-acid molecule is the only form stabilized in the monolayer and multilayer regimes. No ordered adsorption phases form at these temperatures. Adsorption at room temperature also leads to the creation of one chemical form only, in this case, the monotartrate species that is adsorbed onto the surface via its carboxylate functionality, with the opposite end of the molecule retaining its COOH functionality and interacting with neighboring molecules either by an  $\alpha$ -hydroxy group at low coverages or by forming even stronger cyclic dimer interactions at high coverage. These intermolecular forces are responsible for inducing substantial self-organization in the adlayer, leading to a (4 0, 2 3) ordered structure at low temperatures and a (4 1, 2 3) structure at higher coverages. At high temperatures of >400 K and at low coverages, the bitartrate form of *R,R*-tartaric acid is preferred in which both carboxylate groups are bound to the metal surface, attached to Cu atoms on opposite sides of a trough on the (110) surface. Again, significant H-bonding interactions between the  $\alpha$ -hydroxy groups of neighboring molecules leads to the creation of a very ordered (9 0, 1 2) structure. The bitartrate species is the thermodynamically preferred form at low coverages, but its creation is kinetically hindered at low temperatures. At high coverages, the monotartrate form becomes favorable and increased adsorption leads to the conversion of the bitartrate form to the monotartrate form, after which the system then effectively mimics the adsorption route followed at 300 K.

Turning now to the operating catalytic system, we note that the final enantioselective performance of the *R,R*-tartaric acid modified Ni catalyst shows a strong dependence on temperature,<sup>24–27</sup> pH,<sup>25,26,28–31</sup> modifier concentration,<sup>24,25,31</sup> and modification time.<sup>30</sup> Our model studies on Cu(110), for the first time, provide a rationalization of these effects by demonstrating that varying the adsorbate coverage (i.e., concentration), temperature, and adsorbate flux (i.e., time) can have very large effects on the nature of adsorbed species and the 2-dimensional

ordering at the surface. These different adlayers will clearly provide different docking sites for incoming reactant molecules and each structure will play a different role in the enantioselective reaction. Of particular interest is the fact that under certain conditions, the 2-dimensional order of the *R,R*-tartaric acid adlayer destroys all symmetry elements at the surface, leading to the creation of extended chiral surfaces. This bestowing of chirality onto a nonchiral metal surface may be an important factor in defining the active site in heterogeneous enantioselective reactions.

**Acknowledgment.** We are grateful to the EPSRC for equipment grants and postdoctoral fellowships to S.H., T.B., and P.M. We also thank the Leverhulme Centre for Innovative Catalysis for a Ph.D. studentship for M.O.L.

#### References and Notes

- (1) Izumi, Y. *Adv. Catal.* **1983**, *32*, 215.
- (2) Webb, G.; Wells, P. B. *Catal. Today* **1992**, *12*, 319.
- (3) Raval, R.; Baddeley, C. J.; Haq, S.; Louafi, S.; Murray, P.; Muryn, C.; Ortega Lorenzo, M.; Williams, J. In *Reaction Kinetics and the Development of Catalytic Processes*; Froment, G. F., Waugh, K. C., Eds.; Elsevier Science B.V.: Amsterdam, 1999.
- (4) Keane, M. A.; Webb, G. *J. Catal.* **1992**, *136*, 1.
- (5) Tai, A.; Harada, T.; Hiraki, Y.; Murakami, S. *Bull. Chem. Soc. Jpn.* **1983**, *56*, 1414.
- (6) Okaya, Y.; Stemple, N. R.; Kay, M. I. *Acta Crystallogr.* **1966**, *21*, 236.
- (7) Edsall, J. T. *J. Chemical Phys.* **1966**, *5*, 508.
- (8) Gordy, W. *J. Chem. Phys.* **1937**, *5*, 284.
- (9) Badger, R. M.; Bauer, S. H. *J. Chem. Phys.* **1937**, *5*, 605.
- (10) Badger, R. M.; Bauer, S. H. *J. Chem. Phys.* **1937**, *5*, 839.
- (11) Gillette, R. H.; Daniels, F. *J. Am. Chem. Soc.* **1936**, *58*, 1139.
- (12) Greenler, R. G.; Snider, D. R.; Witt, D.; Sorbello, R. S. *Surf. Sci.* **1982**, *118*, 415.
- (13) Bhattacharjee, R.; Jain, Y. S.; Bist, H. D. *J. Raman Spectrosc.* **1989**, *20*, 91.
- (14) Bellamy, L. J. *Advances in Infrared Group Frequencies*; Methuen and Co. Ltd.: London, 1968; p 173.
- (15) Woodruff, D. P.; McConville, C. F.; Kilcoyne, A. L. D. *Surf. Sci.* **1988**, *201*, 228.
- (16) Bao, S.; Liu, G.; Woodruff, D. P. *Surf. Sci.* **1988**, *203*, 89.
- (17) Frederick, B. G.; Leible, F. M.; Haq, S.; Richardson, N. V. *Surf. Rev. Lett.* **1996**, *3* (4), 1523.
- (18) Williams, J.; Haq, S.; Raval, R. *Surf. Sci.* **1996**, *368*, 303.
- (19) Avram, M. *Infrared Spectroscopy—Applications in Organic Chemistry*; Wiley Interscience: New York, 1972; pp 388–398.
- (20) Bellamy, L. J. *The Infrared Spectra of Complex Molecules*; Methuen and Co. Ltd.: London, 1964; pp 161–170.
- (21) Srivastava, G. P.; Mohan, S.; Jain, Y. S. *J. Raman Spectrosc.* **1982**, *13* (1), 25.
- (22) Bhattacharjee, R.; Jain, Y. S.; Raghubanshi, G.; Bist, H. D. *J. Raman Spectrosc.* **1988**, *19*, 51.
- (23) Ortega Lorenzo, M.; Haq, S.; Baddeley, C. J.; Raval, R. Manuscript in preparation.
- (24) Keane, M. A. *Langmuir* **1997**, *13*, 41.
- (25) Tai, A.; Harada, T. In *Tailored Metal Catalysts*; Iwasawa, Y., Ed.; D. Reidel Publishing Co.: Dordrecht, The Netherlands, 1986; pp 265–324.
- (26) Fish, M. J.; Ollis, D. F. *J. Catal.* **1977**, *50*, 353.
- (27) Hoek, A.; Sachtler, W. M. H. *J. Catal.* **1979**, *58*, 276.
- (28) Wittmann, G.; Bartok, G. B.; Bartok, M.; Smith, G. V. *J. Mol. Catal.* **1990**, *60*, 1.
- (29) Harada, T.; Yamamoto, M.; Onaka, S.; Imaida, M.; Ozaki, H.; Tai, A.; Izumi, Y. *Bull. Chem. Soc. Jpn.* **1981**, *54*, 2323.
- (30) Klabunovskii, E. I.; Vedenyapin, A. A.; Chankvetadze, B. G.; Areshidze, G. C. In *Proceedings, 8th International Congress on Catalysis*, Berlin, 1984; Dechema, Frankfurt-am-Main, 1984; Vol. 5, p 543.
- (31) Richards, D. R.; Kung, H. H.; Sachtler, W. M. H. *J. Mol. Catal.* **1986**, *36*, 329.